Environmental Pollution 266 (2020) 115389

Contents lists available at ScienceDirect

Environmental Pollution

journal homepage: www.elsevier.com/locate/envpol

Detection of Hg(II) in adsorption experiment by a lateral flow biosensor based on streptavidin-biotinylated DNA probes modified gold nanoparticles and smartphone reader☆

Zizhang Guo [a, c], Yan Kang [b], Shuang Liang [a], Jian Zhang [a, *]

[a] Shandong Key Laboratory of Water Pollution Control and Resource Reuse, School of Environmental Science and Engineering, Shandong University, Qingdao, 266237, China
[b] College of Environment and Safety Engineering, Qingdao University of Science and Technology, Qingdao, 266042, China
[c] School of Mechanical and Materials Engineering, Washington State University, Pullman, WA, 99164-2920, USA

ARTICLE INFO

Article history:
Received 20 May 2020
Received in revised form
28 July 2020
Accepted 4 August 2020
Available online 9 August 2020

Keywords:
Hg(II)
Detection
Smart-phone
Carbon adsorbent
Removal

ABSTRACT

The increased occurrence of Mercury (Hg II) contaminant has caused environmental and health concerns worldwide. Removal of Hg(II) from water is of significant interest, in particular if these can be coupled in a manner of detection. Here, a novel activated carbon (AC) adsorbent and a fast detection device to form a closed-cycle strategy was developed. The synthesis of conjugates of streptavidin-biotinylated DNA probes modified gold nanoparticle was used with lateral flow biosensors for Hg(II) detection. A quantification was completed via a self-developed smartphone app and its limit of detection was 2.53 nM. Moreover, AC was activated with a new activating agent of diammonium hydrogen phosphate. The adsorbent was characterized and determined to have an amorphous microporous structure with a high surface area (1076.5 m^2 g^{-1}) and demonstrated excellent removal efficiency (99.99%) and adsorption capacity (~100 mg g^{-1}) for Hg(II). The kinetics of the pseudo-second-order model and the mechanisms of electrostatic adsorption, ion exchange, and complex reactions are provided. The proposed closed-cycle strategy can be useful for early, fast, and mobile detection of Hg (II) pollution, followed by its effective removal during water treatment.

1. Introduction

The contamination of water resources with mercury (Hg II), a well-known toxic heavy metal released by industrial effluents, is a major cause of environmental damage and health problems worldwide (Guo et al., 2018; Zandiatashbar et al., 2018). Several events related to mercury poisoning have occurred throughout the years including the Minamata disease in Japan in 1956 (Harada, 1995; Obrist et al., 2017). The threshold of Hg(II) concentration in water is 10 nM according to the U.S. EPA guidelines (EPA, 2005). The persistence of Hg(II) in water hinders its biodegradation and removal in conventional wastewater treatment plants. Hg(II) is enriched in the food chain and can lead to serious health effects even at very low concentrations (Beal et al., 2015; Brocza et al., 2019). Therefore, methods and tools to remove Hg(II) contamination from water are critical yet challenging.

The removal of Hg(II) from aqueous effluents has conventionally been done with techniques such as ion exchange (Dabrowski et al., 2004), mechanical filtration (Fan et al., 2018), chemical precipitation (Ghasemi et al., 2017), reverse osmosis (Roy et al., 2019), flotation (Li et al., 2017), and membrane separation (Chaturabul et al., 2015). However, some of these methods can generate a high quantity of toxic sludge or are not economically feasible in terms of operation and capital cost. Adsorption has received considerable attention in recent years because of advantages compared with traditional methods (Chandra and Kim, 2011). The adsorbent materials are highly efficient, easy to handle, and have shown excellent potential for the removal of Hg(II). Activated carbon (AC) is the most popular and widely used adsorbent due to its excellent performance including high adsorption, low cost, and ease of use (Guo et al., 2019; Liu et al., 2019b). Surface functionalization using novel methods endows the AC with a strong affinity for the target metal ions at optimum conditions to remove Hg(II)

☆ This paper has been recommended for acceptance by Baoshan Xing.
* Corresponding author.
E-mail address: ese207@163.com (J. Zhang).

https://doi.org/10.1016/j.envpol.2020.115389
0269-7491/

Table 1
Sequences of oligonucleotides used in this study.

Name	Sequence (5′-3′)
Thiolated DNA probe	SH/ThioMC6-D/-GCTCGTGGTCCTGG
Test line probe	Biotin /-CCCCCCTGGTCCTCGTGC
Control line probe	Biotin /-CCCCCCAGGACCACGAGC

from water. Particularly, the surface oxygen and nitrogen functional groups of adsorbent can share the electron pair for binding Hg(II) (Guo et al., 2017b). Meanwhile, the intense binding energy was produced between functional groups and Hg(II) based on lewis hard-soft acid-base theory (Chandrakumar and Pal, 2002). Recently, several researchers have explored some functional ACs for Hg(II) removal from water. Saleh et al. (2017) used polyethyleneimine to modify AC to append N-functional groups for enhanced removal of Hg(II). Jin et al. (Gang et al., 2016) found that AC was modified with humic acid showed highly efficient for Hg(II) removal due to the contribution of oxygen-containing functional groups. These methods all go through tedious and complicated steps such as carbonization, activation and modification. Here, we have developed a new activating agent of diammonium hydrogen phosphate (DAP) and prepared AC with rich functional groups in one step.

During the adsorption experiment, traditional methods to detect Hg(II) include Atomic Absorption Spectroscopy, Ion Chromatography, and Inductively Coupled Plasma - Mass Spectrometry (He et al., 2011). However, these methods rely on bulky and complex instruments that are expensive, time-consuming, and require trained personnel. To avoid these defects, simple and rapid methods such as biosensors (Cheng, 2015; Xu et al., 2019), chemical sensors (De la Cruz Guzman et al., 2014), nanosensors (Goncalves et al., 2010; Yao et al., 2019), microcantilever sensors (Selid et al., 2009), and piezoelectric sensors (Ensafi et al., 2008; Liu et al., 2019a) were developed. Inside, lateral flow biosensors (LFB) is a promising technology in the detection of Hg(II) because they are affordable, sensitive, equipment-free, and deliverable to the end-user. Wang et al. (2015) designed a hemin/G-quadruplex-based colorimetric sensor for Hg(II) detection in water, and its limit of detection is approximately 100 nM. Zhu et al. (2018), reported a duplex functional G-quadruplex/NMM fluorescent probe as a donor fluorophore for Hg(II) detection that improved the sensitivity to 18.6 nM. But their limitation of detection is higher than 10 nM and not suitable for Hg(II) detection in water. Herein, a colorimetric method with highly sensitive and selective for Hg(II) detection that relies on thymine-Hg(II)-thymine base-pair conjugated gold nanoparticles (Au-NPs) was proposed. The approach based on the color change due to thymine mismatches of bind the Hg(II) (He et al., 2011). But, there is a drawback with poor color recognition at low concentrations. Therefore, we couple LFBs technology with smartphones to quickly interpret the data on specific Hg(II) concentrations.

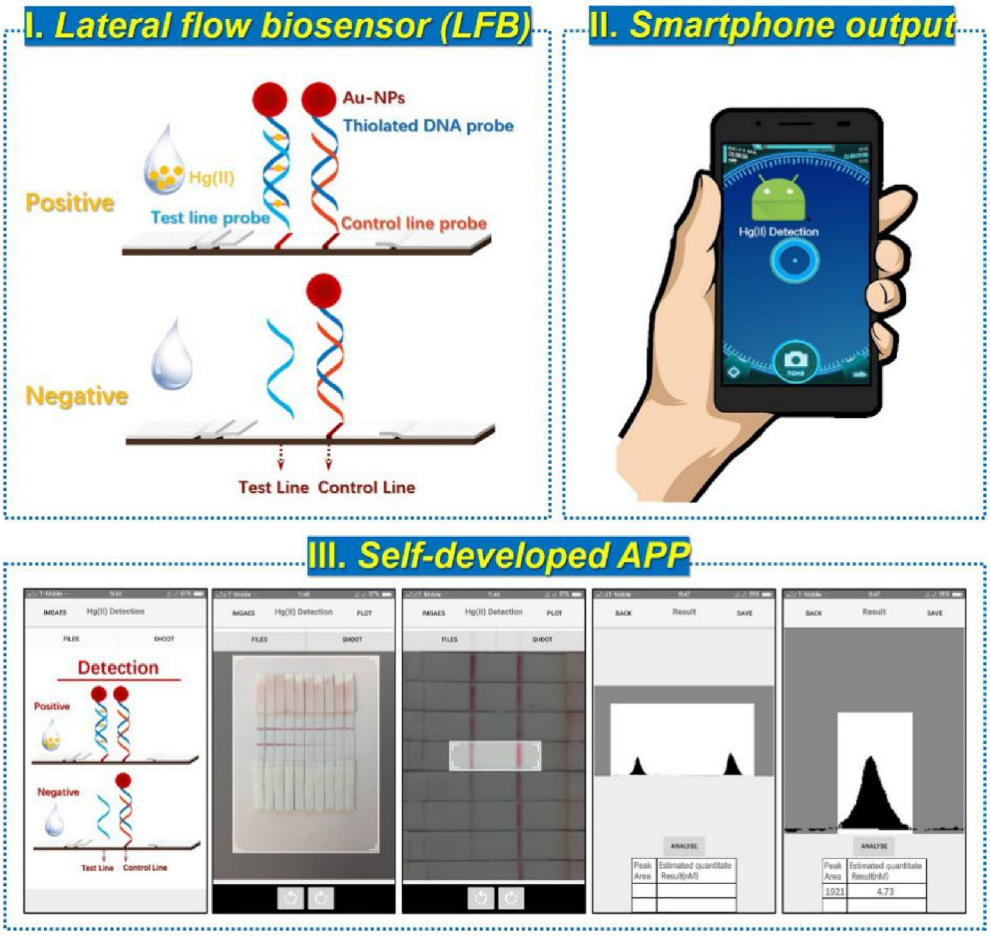

Scheme 1. Schematic of the developed LFB, smartphone output, and self-developed app for Hg(II) detection.

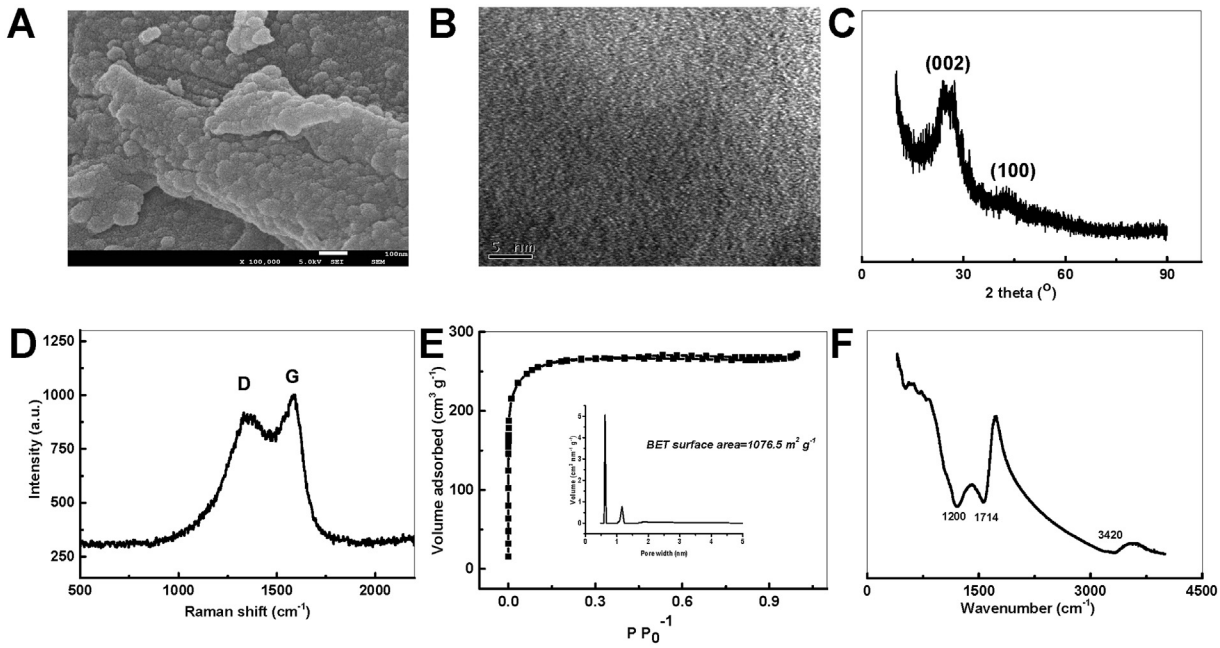

Fig. 1. (A) SEM image, (B) HRTEM micrograph, (C) XRD pattern, (D) Raman spectrum, (E) N2 adsorption/desorption isotherm and pore distribution (insert), and (F) FTIR spectrum of AC.

The objectives of this study were to investigate the physical and chemical properties of the AC prepared by the new activator and to evaluate its Hg(II) adsorption capacity. Meanwhile, the accuracy, sensitivity, and selectivity of the new detection technology were assessed and applied to the study of the adsorption kinetics of Hg(II) by the novel AC. At the same time, X-ray photoelectron spectroscopy (XPS) technology was used to analyze the adsorption mechanism of Hg(II). In summary, a closed-cycle strategy for Hg(II) detection and removal was provided. More importantly, it can be used as a reliable detection and removal technology in Hg environmental pollution emergency events in water bodies.

2. Materials and methods

2.1. Chemicals and materials

All general chemicals and materials (analytically pure grade) were commercially available and used as received. All DNA sequences were purchased by Sangon Biotech Co., Ltd. (Shanghai, China). Streptavidin was purchased from Invitrogen (Carlsbad, CA, USA). Deionized water was used in the adsorption experiments, whereas double distilled water was used in all detection experiments.

2.2. Preparation of AC

The biomass precursor *Phragmites australis* (PA) was collected from the local Lake. After a series of pre-treatment processes such as washing and drying, the PA was mixed with DAP with a mass ratio (g PA: g DAP) of 1:1.5 for 10 h and then dried at 105 °C in a convection oven. The sufficiently impregnated samples were placed in a tube furnace for activation at 700 °C under pure N_2 flow for 1 h. After cooling to room temperature, the output samples were washed to a stable pH. Finally, the carbide was dried at 105 °C overnight and sieved 200 mesh. The resulting activated carbon adsorbent was designated as AC.

2.3. Preparation of LFB

The preparation of LFB includes four steps: synthesis of gold nanoparticles (Au-NPs), modification of Au-NPs by thiolated DNA probe, conjugation of streptavidin-biotinylated probes, and LFB fabrication. Added 1.67 mL of 1% trisodium citrate to 50 mL of boiled 2.4×10^{-4} M $HAuCl_4$ solution and then was stirred for 30 min to synthesize aqueous solution of Au-NPs. Then, 30 μl of 100 mM dATP, 15 μl of 1% SDS and 40 μl of 1 M NaCl were added in 1 mL of Au-NP solution. Each additional reagent required 20 min of incubation at room temperature. And then, 0.5 OD of thiolated DNA probe was added and was incubated for 4 h at 60 °C. After incubation, the mixture was centrifuged and washed to obtain the thiolated DNA probe modified Au-NP. To obtain streptavidin-biotinylated probes, equal amounts of 1 mg/mL of streptavidin and 50 μM DNA probe solution were mixed in PBS containing 0.5% mycose and then were incubated for 1 h at room temperature. The sequences of oligonucleotides used were listed in Table 1. The LFB fabrication was carried out according to the method in the reference (Cheng et al., 2017).

2.4. Characterization methods

A scanning electron microscope (SEM, ZEISS SUPRA 40, Germany) was used to record the surface morphology of the adsorbent. The N_2 adsorption/desorption isotherms were measured by a surface area analyzer (Micro, 2020; USA) to calculate specific surface area and pore size distribution of the adsorbent according to BET and DFT computational models. The X-ray diffraction patterns (XRD) were collected on a Bruker D8 X-ray diffractometer using Cu Kα radiation. The Raman spectra were recorded using a Renishaw in Via 2000 instrument (Renishaw, UK). The Fourier transform infrared (FTIR) spectroscopy of the adsorbent was acquired with a Nicolet-460 (Thermo Fisher Scientific Inc., USA). The Hg(II) removal mechanism was determined by X-ray photoelectron spectra (XPS; Thermo Fisher Scientific Inc., USA) of AC before and after adsorption of Hg(II).

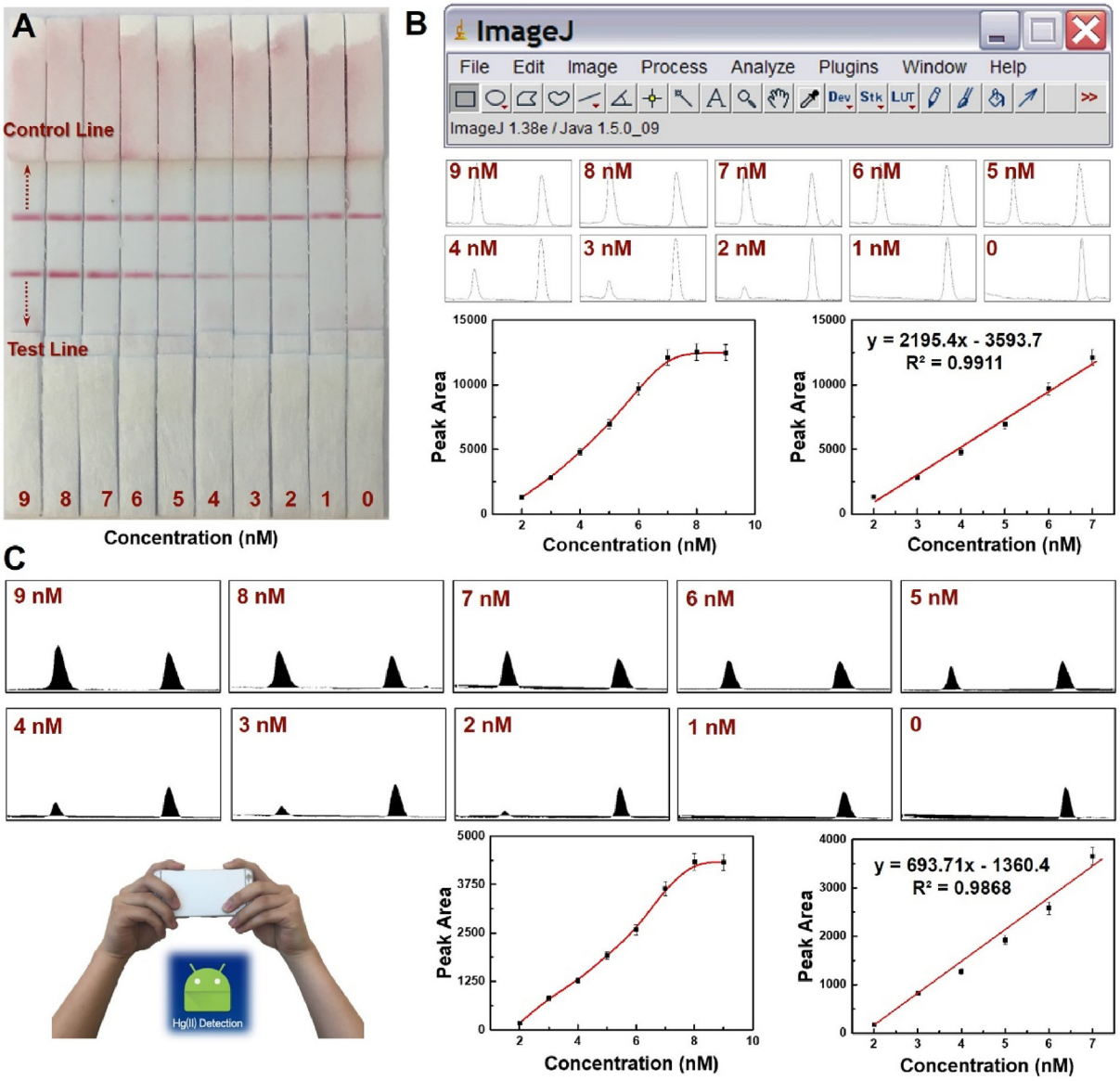

Fig. 2. Sensitivity of the LFB for Hg(II) detection. (A) Photo images of LFBs in response to various concentrations of Hg(II) from left to right: 9 nM, 8 nM, 7 nM, 6 nM, 5 nM, 4 nM, 3 nM, 2 nM, 1 nM, and negative control. The images were recorded with a smartphone camera (12-megapixel). (B) Quantitative detection used ImageJ software. The response curve and calibration curve of the peak areas of test lines versus log Hg(II) concentration (nM). (C) Quantitative detection used a smartphone app. The response curve and calibration curve of the peak areas of the test lines versus Hg(II) concentration (nM). Error bars indicate the standard deviation of three measurements.

Transmission electron microscopy (TEM) images of Au-NPs were acquired with a Tecnai-G20 instrument (Thermo Fisher Scientific Inc., USA). The ultraviolet–visible (UV–vis) absorption spectra of Au-NPs and DNA-modified Au-NPs were obtained with a Tecan Safire II multimode plate reader. The results were shown in Fig. S1, indicating that the probe conjugates were successfully synthesized on Au-NPs.

2.5. Detection of Hg(II)

The application of the LFB sensor to detect Hg(II) followed the subsequent steps. The desired amount of Hg(II) and 50 μL of running buffer were dropped in the sample pad. The DNA probe-modified Au-NP conjugates (2.5 μL) were loaded onto the conjugate pad. And the solution migrated by capillary force with visual observation within 5 min. To facilitate fast detection, an Android app was developed that utilized an 8-megapixel camera based on ImageJ (NIH, MD), which was used for quantitative measurements of the images. By directly taking pictures or selecting pictures, the concentration of Hg(II) from water could be quickly and accurately obtained. The operation steps are shown in Scheme 1.

2.6. Hg(II) adsorption experiment

For the removal studies of Hg(II) over time with AC, 1 g of AC was added to a 1-L beaker containing an aqueous solution with an excessive initial Hg (II) concentration of 100 mg L^{-1}. The solution was stirred at 120 rpm with an electromagnetic stirrer at the initial pH. The Hg(II) concentration was determined with the method described above in Section 2.5. At the same time, the atomic absorption spectrometry (180-80, Hitachi, Japan) was used for the concentration outside the measurement range. The removal efficiency of Hg(II) and the adsorption capacity (Q_e) of AC was calculated as follows:

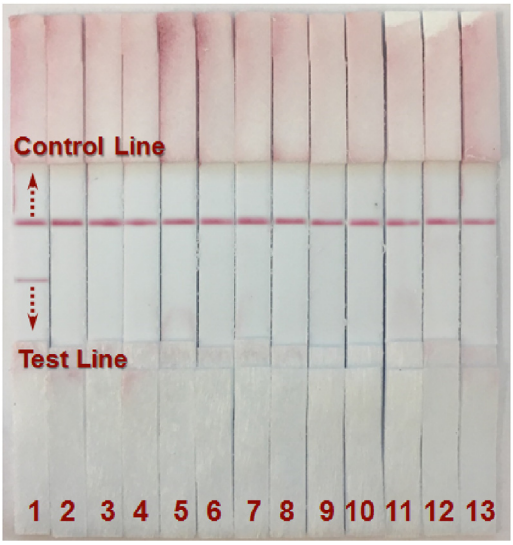

Fig. 3. Selectivity of the LFB for Hg(II) over other potential metal ions. Photo images of LFBs in response to various mental ions: (1) Hg(II); (2) Zn(II); (3) Mg(II); (4) Pb(II); (5) Fe(III); (6) Fe(II); (7) Cu(II); (8) K(I); (9) Ca(II); (10) Mn(II); (11) Ag(I); (12) Au(III) and (13) Ni(II). The concentration of Hg(II) is 5 nM. The concentration of the other metal ion is 1 mM. The images were recorded with a camera phone (12-megapixel).

$$\text{Removal efficiency } (\%) \frac{C_0 - C_e}{C_0} \times 100 \quad \text{Eq. (1)}$$

$$Q_e = (C_0 - C_e) \times V/M \quad \text{Eq. (2)}$$

Here, C_0 and C_e are the initial and equilibrium concentrations of Hg(II) (mg L^{-1}), respectively, V represents the solution volume (L), and M is the weight of AC (g).

3. Results and discussion

3.1. Morphological and characterization of AC

The rough surface and orderly porous structure of the AC, as obtained from SEM and TEM imaging, can be observed in Fig. 1A and B; this is typical of carbon adsorbents (Li et al., 2016). This porous morphology is mainly due to the sculpture of the new DAP activator, as well as the generation of gas and dehydration-condensation of phosphate resulting from the activation process (Guo et al., 2017a). Fig. 1C shows the XRD pattern of the AC adsorbent and the two peaks corresponding to graphite (002) and (100). The asymmetrical (002) peak was presented in the examined range due to the presence of a γ-band. The spectra of the (002) and (100) peaks, as well as the γ-bond, indicate that ordered and disordered carbon structures were present in the adsorbent (Zhao et al., 2009). The Raman spectrum of the adsorbent is shown in Fig. 1D. Two visible peaks were observed at 1583 cm^{-1} (G-band) and 1345 cm^{-1} (D-band) and were recorded between 500 and 2000 cm^{-1}. The G-bond is caused by a plane stretch motion of the 2p carbon atoms (E_{2g} vibrational mode). The D-band relates to A_{1g} symmetry and is attributed to a disordered graphite structure. The valley that exists between the two peaks represents the presence of amorphous carbon in the AC structure (Rajagopal et al., 2016).

Fig. 1E shows the N_2 adsorption/desorption isotherm and pore distribution (insert) of the AC. According to the IUPAC classification, the isotherm is type I, which is characteristic of a microporous structure (Schneider, 1995). The pore distribution confirms the microporosity since most of the pore width is less than 1 nm, while the BET surface area of the adsorbent is 1076.5 m^2 g^{-1}. This feature of the AC contributes to the adsorption of Hg(II) in aqueous solutions because of the smaller ionic radius and the hydrated ionic radius of the metal ions. FTIR spectra investigated the surface functional groups of adsorbents were shown in Fig. 1F. The main

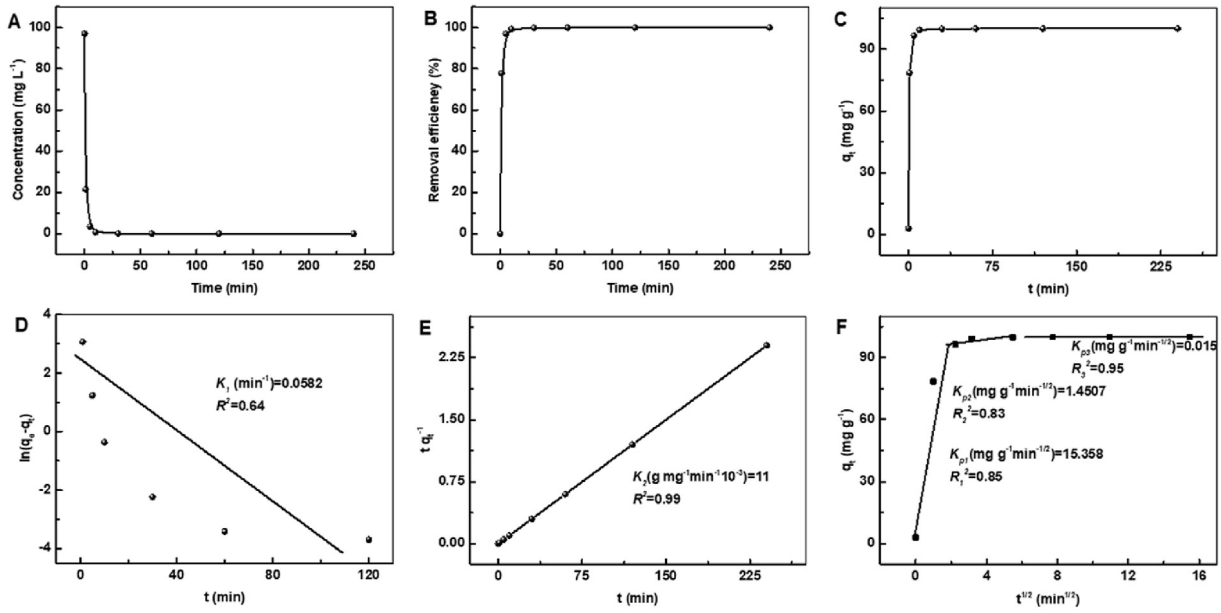

Fig. 4. Effect of contact time for Hg(II) removal on AC: (A) concentration (mg/L), (B) removal efficiency (%), (C) adsorption capacity (mg/g). The linear plots and parameters of the (D) pseudo-first-order model, (E) pseudo-second-order model and (F) intra-particle diffusion plots.

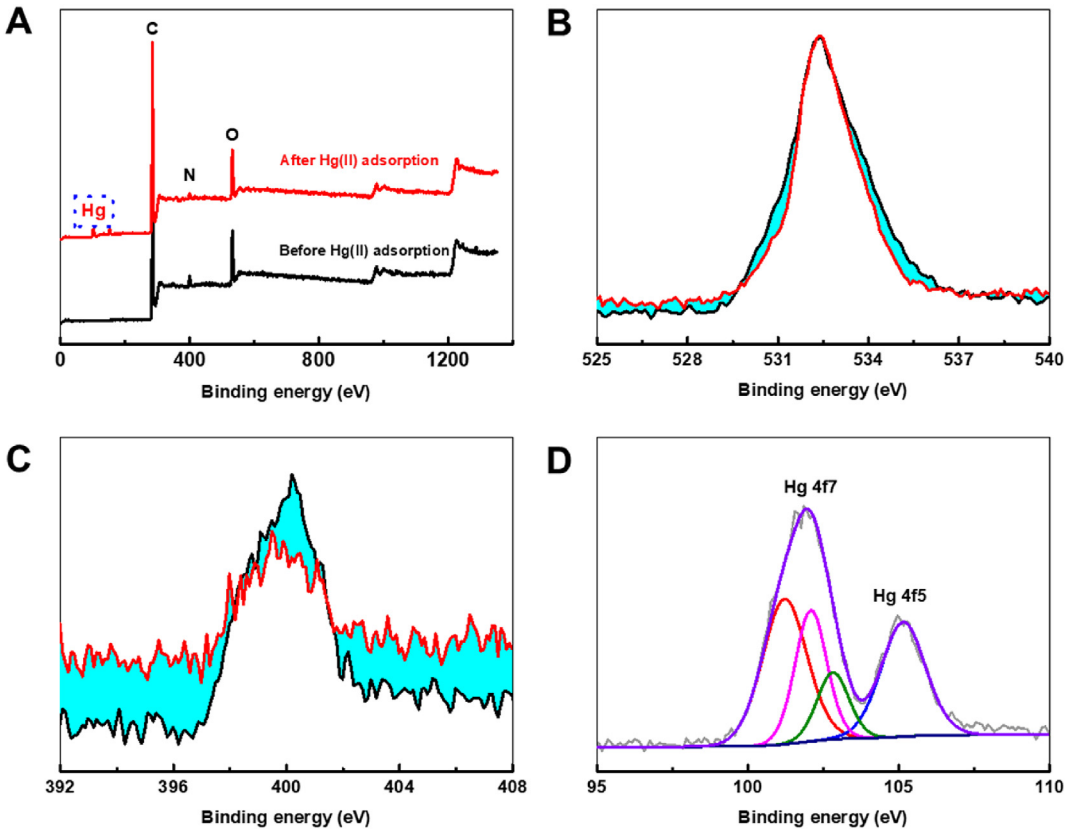

Fig. 5. XPS spectra for carbon adsorbent before and after Hg(II) adsorption: (A) survey spectra, (B) O 1s, (C) N 1s and (D) Hg 4f.

peaks at 1200, 1714, and 3420 cm^{-1} correspond to the C–O/C–N, C=O, and O–H/N–H stretching vibrations, respectively (Shin et al., 1997). These chemical bonds are formed from the activation process and promote Hg(II) removal.

3.2. Detection of Hg(II) with LFB

Fig. 2A shows an image of the response from the biosensors when detecting different Hg (II) concentrations (0–9 nM) with control and test line to determine the sensitivity of the LFB. The color intensity for each test line became stronger as the Hg(II) concentration increased. Fig. 2B and C shows the corresponding graphs as interpreted by ImageJ or a smartphone, respectively. There were no false positives or false negatives throughout the entire range of concentrations tested. The response curve of the peak areas of test lines versus log Hg(II) concentration (nM) was linear from 2 nM to 7 nM, and the limit of detection (LOD) was calculated to be 2.53 nM based on 3.3 × standard deviations of the regression line/slope (see Fig. 2C). The accuracy and low range detection of Hg (II) with the proposed biosensors can be considered suitable for independent quantitative work for real-time detection of environmentally relevant levels of Hg(II) in water.

The selectivity of the LFB biosensor is shown in Fig. 3 via a series of metal ions at 1 mM. A prominent color represents the low concentration of 5 nM of Hg(II) in LFB on the test line, but the blank requires other metal ions. This demonstrates that the prepared LFB has excellent selectivity for Hg(II), which is attributed to the highly specific coordination of the mismatched base pair. The robustness was one of the most important criteria in evaluating the LFB assay, which was assessed by analyzing one sample for six replicate determinations. A sample solution containing 2 nM Hg(II) was used to examine the performance of the LFBs. As shown in Fig. S2, similar responses could be obtained against each determination. The corresponding RSD values of optical responses were calculated to be 6.3%, indicating the acceptable robustness of the rapid detection measurements.

3.3. Adsorption kinetics

Fig. 4 show the reduction in the concentration and the corresponding removal efficiency of Hg(II) over time. In the first 20 min, Hg(II) is rapidly removed by AC and then gradually decreases until reaching equilibrium. At 240 min, the equilibrium concentration of Hg(II) was 4.87 nM (9.77×10^{-4} mg L^{-1}, Fig. 4A, which is far below the standards of the U.S.EPA (EPA, 0.002 mg L^{-1}) for Hg(II) in drinking water. Fig. 4B and C shows that the AC has excellent removal efficiency (99.99%) and adsorption capacity (~100 mg g^{-1}) for Hg(II). The adsorptive performance of the AC is also better than that of other reference adsorbents (Tan et al., 2016; Xu et al., 2016).

The adsorption kinetics and mechanisms were studied to understand better the process of Hg(II) removal with the proposed adsorbent. Pseudo-first-order (Corbett, 1972) and pseudo-second-order (Ho and McKay, 1999) kinetic models were used to fit the data for Hg(II) removal and explain the adsorption kinetics. Fig. 4 present the plots for the Hg(II) removal when fitting the kinetic models. The pseudo-second-order model ($R^2 > 0.99$) resulted in a better fit than the pseudo-first-order model ($R^2 = 0.64$) in this adsorption process. The calculated constants suggest that multiple processes may control the adsorption mechanism, especially the chemisorption process (Ho, 2006; Ho and McKay, 1998). The intraparticle diffusion model was used to discuss the mechanism of Hg(II) diffusion onto the AC. Results show that the adsorption of

Hg(II) contains three steps. The first instantaneous stage involves external surface sorption and a porous filter. The chemisorption proceeded in the second stage, and the final stage reaches equilibrium due to the limited sites for Hg(II) capture.

3.4. XPS evidence for adsorption mechanism

XPS spectra were used to confirm the mechanism of chemisorption (Fig. 5). Fig. 5A shows that after Hg(II) adsorption with AC, the Hg peak appeared in the XPS survey spectrum and was accompanied by a change of peaks for O 1s and N 1s (see Fig. 5B and C). The XPS peak differentiation/imitating analysis of Hg is shown in Fig. 5D. The peaks at 101.3, 102.1, and 102.8 eV correspond to Hg 4f7 and the peak at 105.2 eV corresponds to Hg 4f5 (Behra et al., 2001; Hyland et al., 1990), indicating bonding between oxygen- or nitrogen-containing surface groups and Hg(II) (Cui et al., 2012; Wang et al., 2009). Also, the C 1s, O 1s, and N 1s spectra and the related parameters for AC before and after Hg(II) adsorption are shown in Fig. S3 and Table S1. The variation in the peaks reflect the role of functional groups in Hg(II) adsorption, as described below:

$$R\text{-}O^- + Hg(II)X \leftrightarrow R\text{-}O^-Hg(II)X \quad \text{Eq. (3)}$$

$$R\text{-}COO^- + Hg(II)X \leftrightarrow R\text{-}COO^- Hg(II)X \quad \text{Eq. (4)}$$

$$R{-}NH_2 + Hg(II)X \rightarrow R{-}NH_2\ Hg(II)X \quad \text{Eq. (5)}$$

$$R{-}NH_3^+ + Hg(II)X \rightarrow R{-}NH_2\ Hg(II)X + H^+ \quad \text{Eq. (6)}$$

Here, R represents other components and Hg(II)X represents Hg(II) species. In summary, in addition to physical adsorption by porous filtration, the surface of the adsorbent is mainly chemical adsorption such as electrostatic adsorption, ion exchange and surface complexation. The donated electrons from the adsorbents' functional groups could form or bind with Hg(II).

4. Conclusion

A simple, accurate detection method was successfully used in the adsorption removal experiment of Hg(II) from water. The synthesis of conjugates of streptavidin-biotinylated DNA probes modified with Au-NPs was used with LFB to show excellent selectivity and sensitivity for Hg(II) detection. A smartphone app offers accurate quantitative identification of Hg(II) concentration and eliminates inconvenient and complex test equipment. The activated carbon adsorbent developed herein demonstrated excellent removal efficiency (99.99%) and adsorption capacity (~100 mg g^{-1}) for Hg(II) removal in water. Thus, the proposed closed-cycle strategy can be useful for early detection of Hg (II) pollution followed by its effective removal during water treatment.

Main finding of the work

A lateral flow biosensor with a limit of detection was 2.53 nM was applied Hg(II) adsorption experiment.

CRediT authorship contribution statement

Zizhang Guo: Conceptualization, Methodology, Writing - original draft, Funding acquisition. **Yan Kang:** Methodology, Formal analysis, Data curation. **Shuang Liang:** Funding acquisition. **Jian Zhang:** Supervision, Project administration, Funding acquisition.

Declaration of competing interest

The authors declare that they have no known competing financial interests or personal relationships that could have appeared to influence the work reported in this paper.

Acknowledgments

This work was supported by the National Natural Science Foundation of China (No. 51908326), China Postdoctoral Science Foundation (No. 2018M640632), and Major Innovation Project of Shandong Province (No. 2019JZZY010411). Zizhang Guo (201606220157) would like to acknowledge the fellowship from the China Scholarship Council (CSC).

Appendix A. Supplementary data

Supplementary data to this article can be found online at https://doi.org/10.1016/j.envpol.2020.115389.

References

Beal, S.A., Osterberg, E.C., Zdanowicz, C.M., Fisher, D.A., 2015. Ice core perspective on mercury pollution during the past 600 years. Environ. Sci. Technol. 49, 7641–7647.
Behra, P., Bonnissel-Gissinger, P., Alnot, M., Revel, R., Ehrhardt, J.J., 2001. XPS and XAS study of the sorption of Hg (II) onto pyrite. Langmuir 17, 3970–3979.
Brocza, F.M., Biester, H., Richard, J.-H., Kraemer, S.M., Wiederhold, J.G., 2019. Mercury isotope fractionation in the subsurface of a Hg (II) chloride-contaminated industrial legacy site. Environ. Sci. Technol. 53, 7296–7305.
Chandra, V., Kim, K.S., 2011. Highly selective adsorption of Hg^{2+} by a polypyrrole–reduced graphene oxide composite. Chem. Commun. 47, 3942–3944.
Chandrakumar, K., Pal, S., 2002. A systematic study on the reactivity of Lewis acid–base complexes through the local hard– soft acid– base principle. J. Phys. Chem. A 106, 11775–11781.
Chaturabul, S., Srirachat, W., Wannachod, T., Ramakul, P., Pancharoen, U., Kheawhom, S., 2015. Separation of mercury (II) from petroleum produced water via hollow fiber supported liquid membrane and mass transfer modeling. Chem. Eng. J. 265, 34–46.
Cheng, N., Xu, Y., Huang, K., Chen, Y., Yang, Z., Luo, Y., Xu, W., 2017. One-step competitive lateral flow biosensor running on an independent quantification system for smart phones based in-situ detection of trace Hg(II) in tap water. Food Chem. 214, 169–175.
Cheng, S., 2015. Intense charge transfer surface based on graphene and thymine-Hg(II)-thymine base pairs for detection of Hg(2. Biosens. Bioelectron. 77, 740–745.
Corbett, J.F., 1972. Pseudo first-order kinetics. J. Chem. Educ. 49, 663.
Cui, H., Qian, Y., Li, Q., Zhang, Q., Zhai, J., 2012. Adsorption of aqueous Hg (II) by a polyaniline/attapulgite composite. Chem. Eng. J. 211, 216–223.
Dabrowski, A., Hubicki, Z., Podkościelny, P., Robens, E., 2004. Selective removal of the heavy metal ions from waters and industrial wastewaters by ion-exchange method. Chemosphere 56, 91–106.
De la Cruz Guzman, P.M., Aguilar-Aguilar, A., Banuelos-Frias, A., Chazaro-Ruiz, L.F., Palestino, G., 2014. Hybrid porous silicon- rhodamine B derivative nanostructures as chemical sensor for Hg(II) detection. Ecs Trans. 64, 31–34.
Ensafi, A.A., Meghdadi, S., Allafchian, A., 2008. Highly selective potentiometric membrane sensor for Hg(II) based on bis(benzoyl acetone) diethylene triamine. IEEE Sensor. J. 8, 248–254.
EPA, U., 2005. Regulatory Import Analysis of the Clean Air Mercury Rule: EPA-452. R-05-003.
Fan, L., Zhou, A., Zhong, L., Liu, Y., 2018. Photoinduced reduction of high concentration Hg (II) to Hg2Cl2 from acid wastewater with the presence of fulvic acid under anaerobic conditions. Chemosphere 198, 13–20.
Gang, Jin, Yujin, Eom, Tai, Gyu, Lee, 2016. Removal of Hg(II) from aquatic environments using activated carbon impregnated with humic acid. J. Ind. Eng. Chem. 46–52, 2016.
Ghasemi, E., Heydari, A., Sillanpää, M., 2017. Superparamagnetic Fe_3O_4@ EDTA nanoparticles as an efficient adsorbent for simultaneous removal of Ag (I), Hg (II), Mn (II), Zn (II), Pb (II) and Cd (II) from water and soil environmental samples. Microchem. J. 131, 51–56.
Goncalves, H.M.R., Jorge, P.A.S., Fernandes, J.R.A., Silva, J.C.G.E.D., 2010. Hg(II) sensing based on functionalized carbon dots obtained by direct laser ablation. Sensor. Actuator. B Chem. 145, 702–707.
Guo, Lin, Shixing, Wang, Libo, Zhang, Tu, Hu, Jinhui, 2018. Selective and high efficient removal of Hg^{2+} onto the functionalized corn bract by hypophosphorous acid. J. Clean. Prod. 639–646, 2018.
Guo, Z., Shams, M., Zhu, C., Shi, Q., Tian, Y., Engelhard, M.H., Du, D., Chowdhury, I.,

Lin, Y., 2019. Electrically switched ion exchange based on carbon-polypyrrole composite smart materials for the removal of ReO_4^- from aqueous solutions. Environ. Sci. Technol. 53, 2612–2617.
Guo, Z., Zhang, J., Liu, H., Kang, Y., 2017a. Development of a nitrogen-functionalized carbon adsorbent derived from biomass waste by diammonium hydrogen phosphate activation for Cr (VI) removal. Powder Technol. 318, 459–464.
Guo, Z., Zhang, J., Liu, H., Kang, Y., Yu, J., Zhang, C., 2017b. Optimization of the green and low-cost ammoniation-activation method to produce biomass-based activated carbon for Ni (II) removal from aqueous solutions. J. Clean. Prod. 159, 38–46.
Harada, M., 1995. Minamata disease: methylmercury poisoning in Japan caused by environmental pollution. Crit. Rev. Toxicol. 25, 1–24.
He, Y., Zhang, X., Zeng, K., Zhang, S., Baloda, M., Gurung, A.S., Liu, G., 2011. Visual detection of Hg^{2+} in aqueous solution using gold nanoparticles and thymine-rich hairpin DNA probes. Biosens. Bioelectron. 26, 4464–4470.
Ho, Y.-S., 2006. Review of second-order models for adsorption systems. J. Hazard Mater. 136, 681–689.
Ho, Y.-S., McKay, G., 1999. Pseudo-second order model for sorption processes. Process Biochem. 34, 451–465.
Ho, Y., McKay, G., 1998. A comparison of chemisorption kinetic models applied to pollutant removal on various sorbents. Process Saf. Environ. 76, 332–340.
Hyland, M., Jean, G., Bancroft, G., 1990. XPS and AES studies of Hg (II) sorption and desorption reactions on sulphide minerals. Geochem. Cosmochim. Acta 54, 1957–1967.
Li, B., Dai, F., Xiao, Q., Yang, L., Shen, J., Zhang, C., Cai, M., 2016. Nitrogen-doped activated carbon for a high energy hybrid supercapacitor. Energy Environ. Sci. 9, 102–106.
Li, J., Song, K., Liu, D., Zhang, X., Lan, Z., Sun, Y., Wen, S., 2017. Hydrolyzation and adsorption behaviors of SPH and SCT used as combined depressants in the selective flotation of galena from sphalerite. J. Mol. Liq. 231, 485–490.
Liu, X., Yao, Y., Ying, Y., Ping, J., 2019a. Recent advances in nanomaterial-enabled screen-printed electrochemical sensors for heavy metal detection. Trends Anal. Chem. 115, 187–202.
Liu, Z., Adewuyi, Y.G., Shi, S., Chen, H., Li, Y., Liu, D., Liu, Y., 2019b. Removal of gaseous Hg0 using novel seaweed biomass-based activated carbon. Chem. Eng. J. 366, 41–49.
Obrist, D., Agnan, Y., Jiskra, M., Olson, C.L., Colegrove, D.P., Hueber, J., Moore, C.W., Sonke, J.E., Helmig, D., 2017. Tundra uptake of atmospheric elemental mercury drives Arctic mercury pollution. Nature 547, 201.
Rajagopal, R.R., Aravinda, L., Rajarao, R., Bhat, B.R., Sahajwalla, V., 2016. Activated carbon derived from non-metallic printed circuit board waste for supercapacitor application. Electrochim. Acta 211, 488–498.
Roy, C., Dutta, A., Mahapatra, M., Karmakar, M., Roy, J.S.D., Mitra, M., Chattopadhyay, P.K., Singha, N.R., 2019. Collagenic waste and rubber based resin-cured biocomposite adsorbent for high-performance removal (s) of Hg (II), safranine, and brilliant cresyl blue: a cost-friendly waste management approach. J. Hazard Mater. 369, 199–213.
Saleh, T.A., Sarı, A., Tuzen, M., 2017. Optimization of parameters with experimental design for the adsorption of mercury using polyethylenimine modified-activated carbon. J. Environ. Chem. Eng. 5, 1079–1088.
Schneider, P., 1995. Adsorption isotherms of microporous-mesoporous solids revisited. Appl. Catal. Gen. 129, 157–165.
Selid, P.D., Xu, H., Collins, E.M., Facecollins, M.S., Zhao, J.X., 2009. Sensing mercury for biomedical and environmental monitoring. Sensors 9, 5446–5459.
Shin, S., Jang, J., Yoon, S.-H., Mochida, I., 1997. A study on the effect of heat treatment on functional groups of pitch based activated carbon fiber using FTIR. Carbon 35, 1739–1743.
Tan, G., Sun, W., Xu, Y., Wang, H., Xu, N., 2016. Sorption of mercury (II) and atrazine by biochar, modified biochars and biochar based activated carbon in aqueous solution. Bioresour. Technol. 211, 727–735.
Wang, J., Deng, B., Chen, H., Wang, X., Zheng, J., 2009. Removal of aqueous Hg (II) by polyaniline: sorption characteristics and mechanisms. Environ. Sci. Technol. 43, 5223–5228.
Wang, W., Kang, T., Chan, P.W.H., Lu, J., Chen, X., Leung, C., Ma, D., 2015. A label-free G-quadruplex-based mercury detection assay employing the exonuclease III-mediated cleavage of T–Hg^{2+}–T mismatched DNA. Sci. Technol. Adv. Mater. 16, 065004-065004.
Xu, C., Ying, Y., Ping, J., 2019. Colorimetric aggregation assay for kanamycin using gold nanoparticles modified with hairpin DNA probes and hybridization chain reaction-assisted amplification. Microchim. Acta 186, 1–7.
Xu, X., Schierz, A., Xu, N., Cao, X., 2016. Comparison of the characteristics and mechanisms of Hg (II) sorption by biochars and activated carbon. J. Colloid Interface Sci. 463, 55–60.
Yao, Y., Jiang, C., Ping, J., 2019. Flexible freestanding graphene paper-based potentiometric enzymatic aptasensor for ultrasensitive wireless detection of kanamycin. Biosens. Bioelectron. 123, 178–184.
Zandiatashbar, N., Ensafi, A.A., Ahoor, A.H., 2018. Magnetic Fe_2CuO_4/rGO nanocomposite as an efficient recyclable catalyst to convert discard tire into diesel fuel and as an effective mercury adsorbent from wastewater. J. Clean. Prod. 172, 68–80.
Zhao, J., Yang, L., Li, F., Yu, R., Jin, C., 2009. Structural evolution in the graphitization process of activated carbon by high-pressure sintering. Carbon 47, 744–751.
Zhu, Q., Liu, L., Xing, Y., Zhou, X., 2018. Duplex functional G-quadruplex/NMM fluorescent probe for label-free detection of lead (II) and mercury (II) ions. J. Hazard Mater. 355, 50–55.